GUERRA, CONFINI E DIRITTI UMANI. LE GEOGRAFIE GIURIDICHE DELLA CORTE EUROPEA DEI DIRITTI DELL'UOMO

Boundary Layer Effects on Experimental Impedance Eduction

Nicolas T. Quintino*, Lucas A. Bonomo†, Lucas M. Pereira‡ and Julio A. Cordioli§
Federal University of Santa Catarina, 88040-900, Florianópolis, Brazil

Francesco Avallone¶
Politecnico di Torino, 10129, Torino, Italy

The experimental characterization of acoustic liners is usually performed using different techniques to evaluate the liner acoustic impedance under conditions similar to those of a turbofan engine. A recent comparison between different experimental test rigs presented divergent results for the acoustic resistance in the presence of grazing flow. The main differences between these test rigs are the duct geometry and the boundary layer profile. Early studies have shown that the boundary layer profile can have a significant impact on the impedance of acoustic liners. In this work, the boundary layer displacement thickness will be varied by changing the configuration of the UFSC test rig to assess its effect on the acoustic impedance for a fixed geometry. Two alternative configurations were tested and resulted in different flow profiles: one with a higher displacement thickness and other with a lower one. A semiempirical model accounting for the flow induced resistance is also compared with the experimental results. Impedance results show an impact on the experimental impedance for higher displacement thickness values, but no impact is observed for lower ones. Results suggest that the semiempirical model accurately predicts the behavior of higher values of boundary layer displacement thickness, but fails for low values of displacement thickness.

I. Introduction

Acoustic liners are passive devices used to attenuate tonal noise components in turbofan engines. Such devices are commonly composed of a honeycomb structure between a rigid backplate and a perforated facesheet, and are typically represented by their acoustic impedance, which can be used in simulations of the aircraft engine noise as a boundary condition. The acoustic impedance is known to depend on liner geometry, Sound Pressure Level (SPL), grazing flow velocity, and boundary layer profile [1–3].

Experimental determination of the liner impedance must be performed in test rigs under operational conditions similar to the nacelle environment. Consequently, Impedance eduction techniques were developed to characterize acoustic liners in realistic conditions[4]. These methods generally rely on measurements of the acoustic field inside a instrumented duct to obtain the acoustic impedance, in which the liner is exposed to the grazing flow and the sound field.

Recently, comparisons between results obtained in different test rigs for the same liner sample have been published. One example is the International Forum for Aviation Research for Aviation Research (IFAR) collaboration project, which proposed a challenge to gather data from different test rigs with liner samples fabricated by 3D printing [5–7]. However, the main focus of these works was on possible differences on geometry caused by different 3D printing equipment. Bonomo et al. [8] performed comparisons between tests performed at the Federal University of Santa Catarina (UFSC) and at the NASA Langley Research Center with 3D printed samples manufactured by the same vendor. Similar impedance results for the no-flow case confirmed the similarity of the samples. However, in the presence of grazing flow, the resistances obtained at UFSC were considerably higher. When comparing the impedances educed with the Goodrich semiempirical model [9], the boundary layer displacement thickness was found to have significant contribution on the discrepancies found. This is aligned with the work of Kooi and Sarin [1], who evaluated the influence of the boundary layer profile on the impedance showing similar trends to those observed by Bonomo et al. [8], but only for the in-situ technique. The influence on impedance eduction techniques of the boundary layer profile has not been previously investigated.

*MSc Student, Laboratory of Vibrations and Acoustics, nicolas.quintino@lva.ufsc.br, AIAA Student Member.
†PhD Student, Laboratory of Vibrations and Acoustics, lucas.bonomo@lva.ufsc.br, AIAA Student Member.
‡PhD Student, Laboratory of Vibrations and Acoustics, lucas.meirelles@lva.ufsc.br, AIAA Student Member.
§Associate Professor, Departament of Mechanical Engineering, julio.cordioli@ufsc.br, AIAA Member.
¶Full Professor, Dimeas Departament, francesco.avallone@polito.it, AIAA Member.

The main goal of the present work is to assess the effect of boundary layer displacement thickness on the liner acoustic impedance. To achieve this, the liner sample section of the UFSC test rig will be placed in different locations and a flow conditioner will be used to achieve distinct boundary layer profiles while maintaining the same bulk Mach number in the test section. By using the UFSC test rig, we will avoid influence of the duct geometry and observe only the effect of the boundary layer. Detailed flow profile measurements will be performed to determine the boundary layer parameters of interest. A direct impedance eduction method based on the Prony method will be used to evaluate the liner impedance. The same 3D printed liner sample used by the authors recent work [8] will be considered under the same operational conditions. A detailed analysis of the results will be provided, including comparisons with previous results from UFSC and NASA, to see if a better agreement between test rigs is obtained in the presence of grazing flow. The agreement between the semiempirical model's grazing flow induced resistance term and the experimental results will also be evaluated.

This document is structured as follows. Section II describes the impedance eduction technique used in this work. Section III presents a description of the UFSC Liner Impedance Test Rig and the flow profile measurements, and also presents the Goodrich semiempirical perforate liner impedance model, highlighting the grazing flow induced resistance term. The results are presented in Section IV. Finally, Section V presents the conclusions.

II. Impedance Eduction

In this work, we will assume the test rig as a bi-dimensional duct. Assuming temporal dependence in the form of $\exp(\mathrm{i}\omega t)$, the acoustic propagation can be modeled by the Convected Helmholtz Equation, which is given by

$$\left(\mathrm{i}k + M\frac{\partial}{\partial z}\right)^2 p - \frac{\partial^2 p}{\partial x^2} - \frac{\partial^2 p}{\partial z^2} = 0, \tag{1}$$

where p is the complex acoustic pressure, $k = \omega/c_0$ is the free-field wavenumber, ω is the angular frequency, c_0 is the speed of sound, $M = U/c_0$ is the flow bulk Mach number and U is the flow velocity, with Cartesian coordinates x and z in the transverse and axial directions, respectively.

In the lined section of the duct, the bottom wall ($x = 0$) has impedance Z, while the upper wall ($x = H$, where H is the duct height) is rigid. The normal component of the acoustic particle velocity vanishes in the presence of a rigid wall, such that the boundary condition is given by $\partial p/\partial x = 0$. For the lined wall, the diffraction in the boundary layer is taken into account by means of the Ingard-Myers boundary condition [10, 11]. Considering these boundary conditions leads to the eigenvalue problem

$$\alpha_n \tan(\alpha_n H) - \frac{Z_0}{\mathrm{i}kZ}\left(\mathrm{i}k - \mathrm{i}M\zeta_n\right)^2 = 0, \tag{2}$$

where α_n are the transverse wavenumbers and ζ_n the axial wavenumbers, $Z_0 = \rho_0 c_0$ is the air characteristic impedance, ρ_0 is the air density and the dispersion relation is given by

$$\alpha_n^2 = (k - M\zeta_n)^2 - \zeta_n^2. \tag{3}$$

Hence, once the axial wavenumber is known, it is straightforward to calculate the liner impedance by solving the system of equations obtained from Eqs. (2) and (3).

In order to extract the axial wavenumber, one can use Prony-like algorithms to fit a sum of damped complex exponentials to the measured acoustic pressure at uniformly spaced locations[4]. In this case, the acoustic pressure at the flush-mounted microphones at the wall opposite to the liner sample is given by

$$p_j = \sum_{n=1}^{\infty} A_n \exp(-\mathrm{i}\zeta_{n,j}\Delta z)^j + w_j \quad \text{for } j = 0, ..., \mathcal{M} - 1, \tag{4}$$

where p_j is the pressure at the j-th microphone, Δz is the distance between two consecutive microphones, w_j is the measurement noise, and $\mathcal{M}$ is the number of microphones.

One main issue of using the original Prony's algorithm, as proposed by Jing et al. [4], is its poor performance in the presence of noise w_j [12]. As an alternative, the Kumaresan and Tufts (KT) algorithm [12], has been successfully applied [13, 14], providing lower uncertainty levels by selecting a reduced number of wavenumbers (propagating modes)[15]. The KT algorithm is used to extract the axial wavenumbers from measured acoustic fields, then the least attenuated mode is selected, which is normally associated with the mode containing the most acoustic energy. A detailed explanation of the method used here can be found in Bonomo et al. [15].

III. Experimental Setup

A. UFSC Liner Impedance Test Rig

The UFSC Liner Impedance Test Rig is a grazing flow acoustic impedance facility composed of modular rectangular ducts with cross-section of $40 \times 100\,\text{mm}^2$. A 3-dimensional schematic view of the test rig is shown in Fig. 1. Quasianechoic terminations at the test rig inlet and outlet minimize acoustic reflections. Eight Beyma CP-855nD compression drivers are distributed both upstream and downstream of the liner test sample holder, in order to generate sound fields up to 150 dB propagating both toward and against the flow. Grazing flow is supplied by an external compressed air system, which is able to sustain a cross-section averaged flow up to Mach 0.7. A KIMO CP-115 differential pressure transmitter is connected to a 2 mm diameter pitot tube located at the test rig inlet. This pitot tube is used to control the flow speed by using a precalibrated factor, obtained using the quadrature method present in the standard ISO 3966:2008[16]. Temperature is monitored with a KIMO TM-110 temperature transmitter at the test rig inlet.

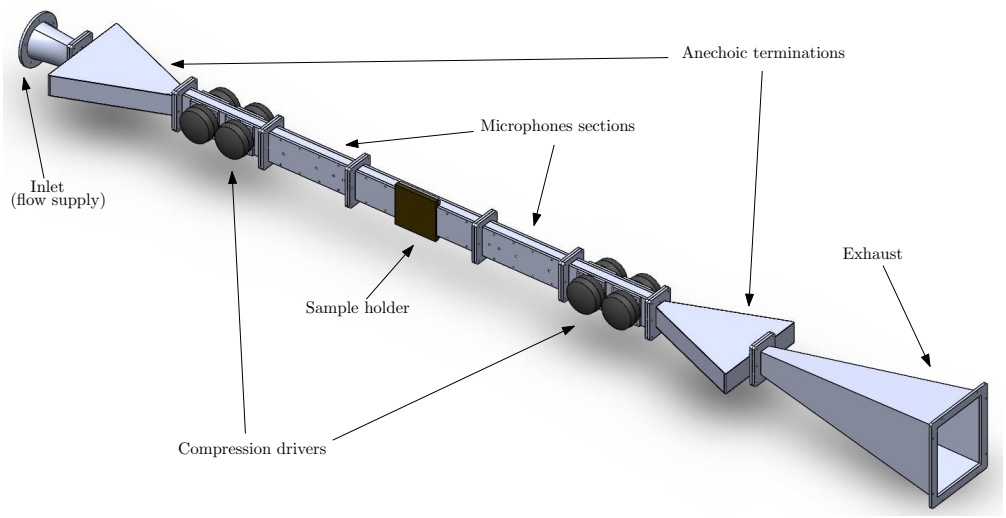

Fig. 1 Schematic representation of the UFSC Liner Impedance Test Rig.

An array of eight equally-spaced flush-mounted B&K DeltaTron 4944 1/4" pressure field microphones is located on the wall opposite to the liner section for impedance eduction. Signals are recorded with a National Instruments PXIe-4499 daq module at a sampling rate of 25.6 kHz. Measurements are performed using the excitation signal as reference for cross-spectrum estimation using Welch's method with 30 averages of 25 600 samples with 75 % overlap. In-house Python3 codes are used for all hardware control, signal processing and post-processing of the data.

B. Flow Profile Measurements

A micrometer linear table is used to translate a Pitot tube to selected positions at the center of the duct. An United Sensor (type BR-025) Pitot tube 0.635 mm diameter is used for the measurement of the flow profile. It has a specific construction shaped for measurements near the walls, which can better characterize the boundary layer. Measurements are performed at the liner sample's upstream edge position, considering 35 positions between the liner wall and the opposite wall, with higher resolution near the walls of the duct. The boundary layer displacement thickness is calculated directly from the experimental points. This is obtained from the points at the liner side of the test rig, from the liner wall ($x = 0\,\text{mm}$) to the center of the duct ($x = 20\,\text{mm}$).

The modular construction of the test rig allows the relocation of the liner sample section upstream and downstream of its original position, changing the boundary layer parameters of the grazing flow over the liner. Also, a flow conditioner was built following the standard ISO 12767:2007[17] as an additional strategy to change the boundary layer. The average Mach number shall also be observed for the different configurations, as it should remain the same. For that, a quadrature method is applied by measuring points along the duct cross-section[16]. A Log-Chebyshev distribution with 5 points per direction is employed, resulting in a total of 25 points with the same weight.

C. Goodrich Semiempirical Model

The Goodrich semiempirical liner impedance model is used in this work to evaluate the impact of changes in the boundary layer displacement thickness, and it is presented in more detail in Yu et al. [9]. The basic expression for this model is given by

$$Z = Z_{\text{of}} + S_{\text{r}} u_0 + R_{\text{cm}} + \text{i}\left(S_{\text{m}} u_0 - \cot\left(kh\right)\right), \tag{5}$$

where Z_{of} is the perforate plate impedance, S_{r} is the nonlinear resistance slope, u_0 is the root-mean-squared acoustic particle velocity, R_{cm} the normalized grazing flow induced acoustic resistance, S_{m} the nonlinear mass reactance and h the liner cavity height.

A correction is applied for liners with a relevant partition wall thickness, which is the case for the liner considered in this study. The main difference caused by this correction is the predicted reactance, resulting in a better agreement with experiments. The $-\cot\left(kh\right)$ term is replaced by the impedance of the core of the liner sample. The core impedance is calculated by the Zwikker and Kosten Transmission Line (ZKTL) model, and the partition wall effects are included using the active area and the total area of a cavity. A complete description of this correction is provided by Jones and Nark [18].

The normalized grazing flow induced acoustic resistance term is analyzed more carefully in this work. It was proposed by Heidelberg et al. [19], and is defined as

$$R_{\text{cm}} = \frac{M}{\sigma\left(2 + 1.256\dfrac{\delta^*}{d}\right)}, \tag{6}$$

where δ^* is the flow profile boundary layer displacement thickness and d is the perforate plate hole diameter. This term has a significant impact on impedance in the presence of grazing flow, and small changes in the value of the boundary layer displacement thickness cause significant differences.

D. Test Matrix and Liner Samples

The liner sample used on this work was manufactured via stereolithography additive manufacturing. The liner sample was designed as an array of individual 9.9×9.9 mm^2 square chambers 38.1 mm high. A total of 8 holes with a diameter $d = 0.99$ mm at the facesheet of each cavity, resulting in a single chamber percentage of open area of approximately 6.3 %. The facesheet thickness is $t = 0.635$ mm. The cell walls are 2.54 mm thick, which gives an overall percentage of open area of 4.2 %. The UFSC sample consists of an array of 8×33 cells, with a total length of 420 mm. Since no backplate was 3D printed in the sample, a 6.35 mm thick aluminum plate was used as the liner sample backplate. The sample can be seen in Fig. 2.

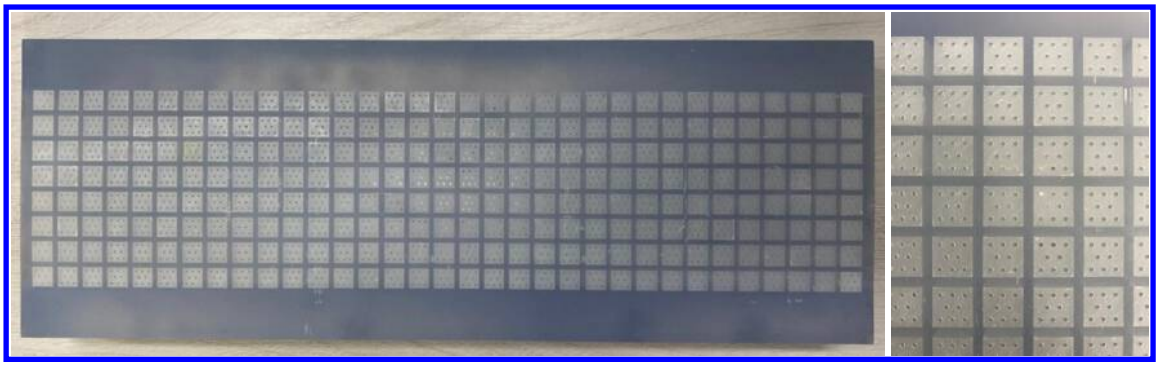

(a) Top view. **(b) Detail of the facesheet.**

Fig. 2 UFSC 3D printed test sample.

Tests were conducted in the absence of flow and with the average Mach number of $M_{\text{avg}} = 0.258$, resulting in centerline Mach number of $M_{\text{center}} = 0.3$ for the default configuration. A stepped pure tone excitation was used, in a set of discrete frequencies ranging from 500 Hz to 2500 Hz with 100 Hz steps. The incident sound pressure level was set at 130 dB, with the acoustic source located upstream or downstream (one at a time) of the liner.

IV. Results and Discussion

A. Default Configuration

The first configuration tested was the original assembly of the test rig. The inlet of the test rig is considered to be the point after a transition from a circular to rectangular duct, so the sections listed for each configuration are just after this point. Fig. 3 presents an schematic of this configuration, for which three sections were positioned before the sample section, namely, the anechoic termination, the loudspeaker section and the microphones section. This configuration presents sightly different results than the previously presented in Bonomo et al. [8], since minor modifications were made at the inlet of the test rig and improvements were made on the flow profile measurement system.

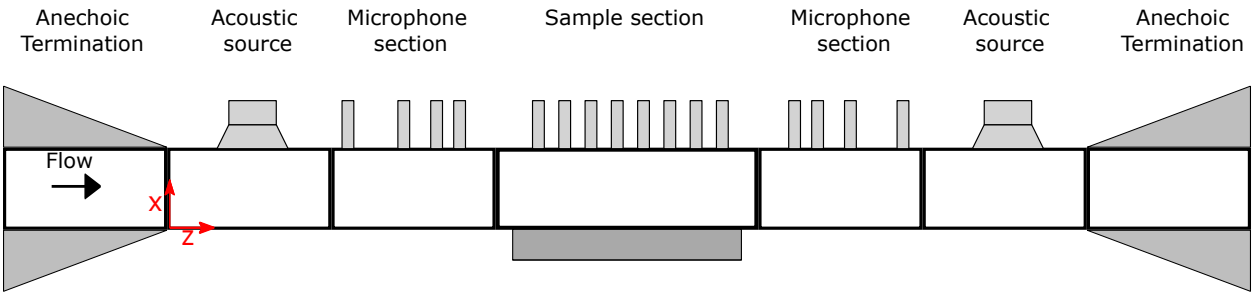

Fig. 3 Schematic of the default configuration.

The flow profile measured for the default configuration is presented in Fig.4. Results at the center of duct are close to the target centerline Mach number of 0.3. This configuration resulted in an average Mach number of approximately 0.258 and a boundary layer displacement thickness of $\delta^* = 1.65$ mm. These are the input values used for the semiempirical model later for the acoustic impedance results. The flow in the test rig was found to be fully developed, as moving the testing section further downstream barely changed the velocity profile.

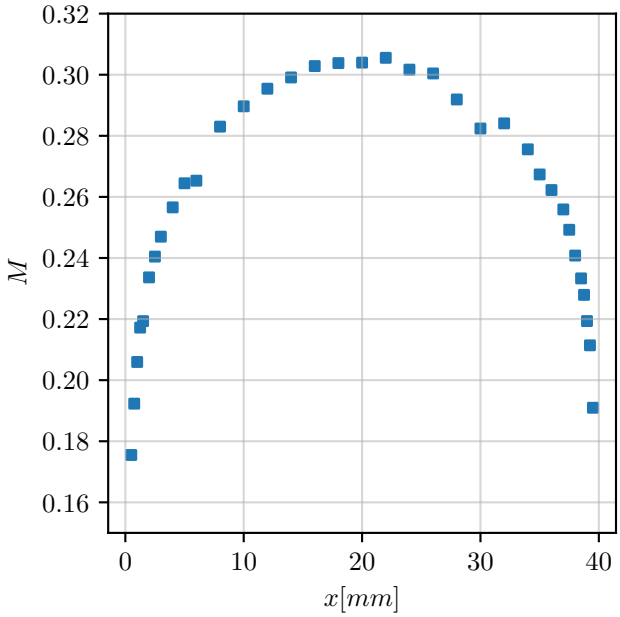

Fig. 4 Flow profile obtained for the default configuration.

Fig. 5 shows the impedance results obtained for the first configuration. These results are for a centerline Mach number of 0.3 and an incident SPL of 130 dB. A good match is observed between the experimental and model resistances for the upstream source case. The downstream source resistance only approaches the model at higher frequencies. This results demonstrate the differences obtained for the upstream and downstream source, as reported in previous works [13, 20].

For the reactance, good agreement with the model is observed, the typical mismatch upstream/downstream remains present.

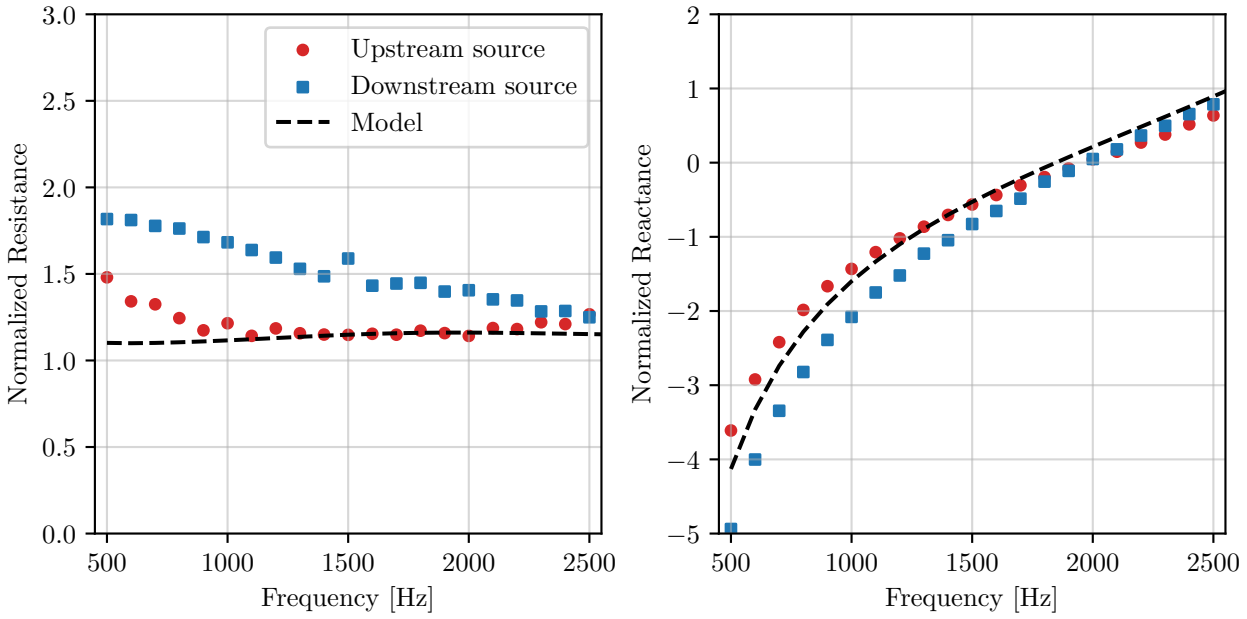

Fig. 5 Impedance results for the default configuration.

B. Flow Conditioner Configuration

The second configuration has a flow conditioner at the beginning of the test rig to change the boundary layer. Before the sample section there are only 2 other components, being the flow conditioner and the acoustic source. An schematic view is presented in Fig. 6. Two other sections were removed when comparing to the previous configuration, i.e., the anechoic termination and the microphone sections. It is worth to highlight that the hard-walled microphone sections do not play a major role in this study, since only the the microphones on the opposite wall of the liner are used for the impedance eduction procedure adopted here (KT). The removal of these sections was the configuration, that caused the higher impact on the flow profile, while still allowing for measure with the upstream and downstream source.

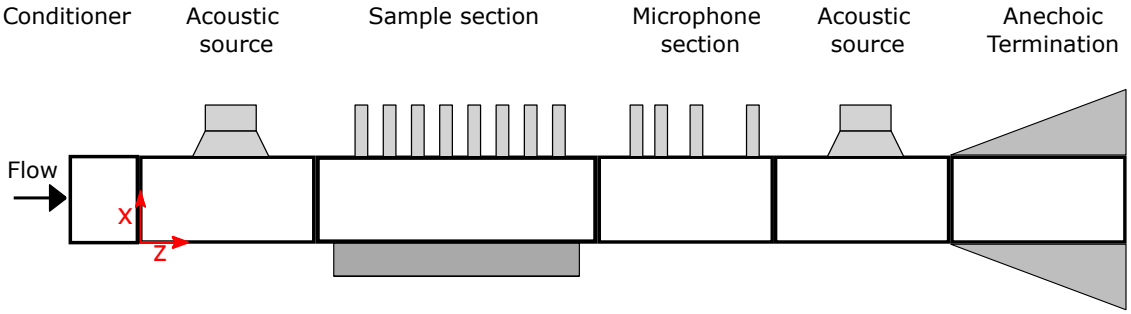

Fig. 6 Schematic of the flow conditioner configuration.

Fig. 7 presents the flow profile measurements for both, the default and the flow conditioner configurations. The same 2D average Mach number was kept in the two configurations, considering the whole duct cross-section. Small differences can be noted near the lined wall, with the higher velocities found for the configuration with the conditioner, when compared with the default configuration. Some discrepancies are found closer to the opposite wall, which made the flow profile asymmetric when the conditioner was considered. The input values for the semiempirical model related to this case are $M_{\text{avg}} = 0.258$ and $\delta^* = 1.8\,\text{mm}$.

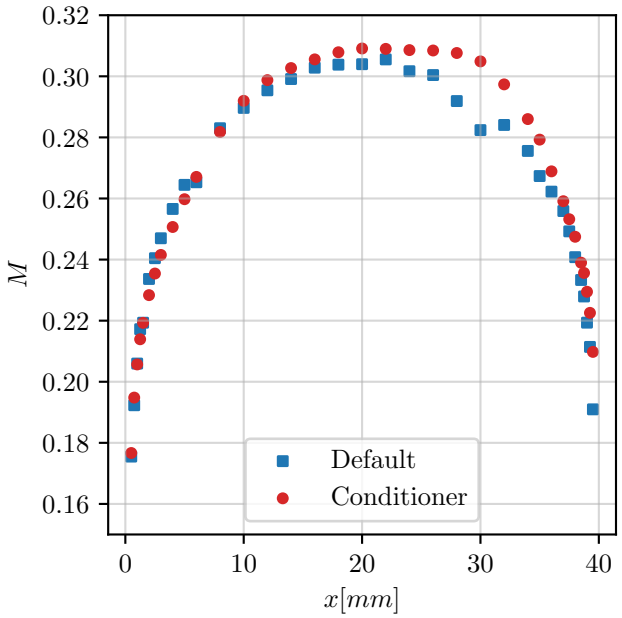

Fig. 7 Flow profiles obtained for the default and the flow conditioner configuration.

Impedance results for the no flow case are presented in Fig. 8. These results show great agreement between the impedances educed with both configurations, which confirms that the changes made in the test rig did not have a major impact on the acoustic field inside the test rig in the absence of flow. Good match is observed between the experimental reactance results and the model.

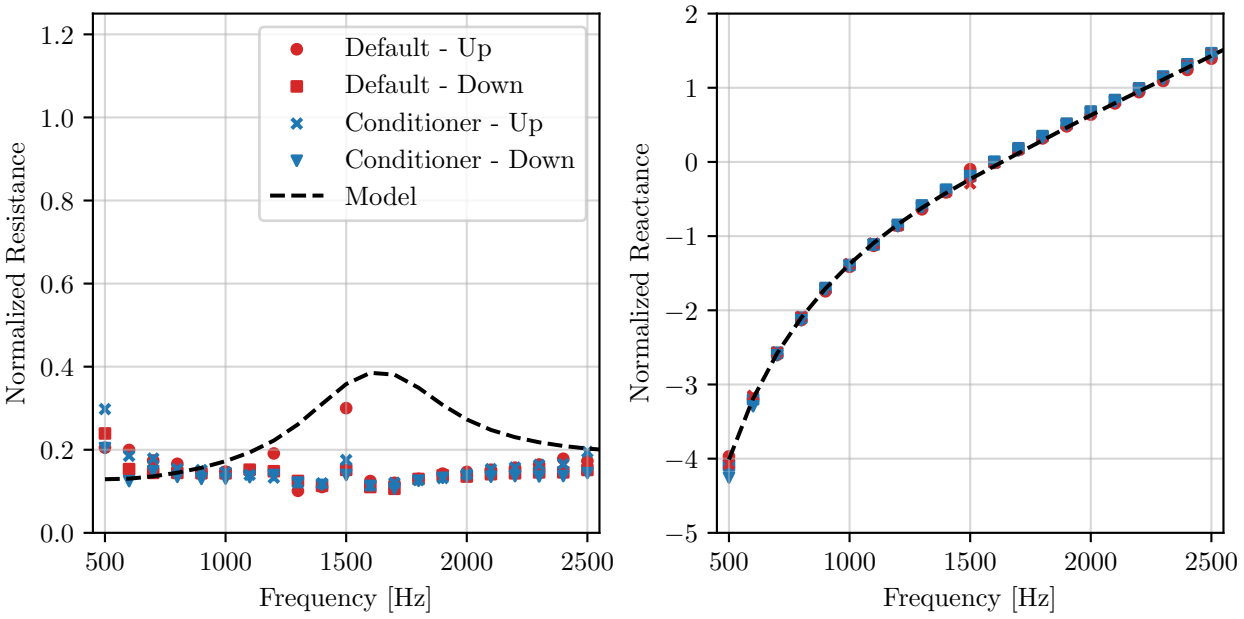

Fig. 8 Impedance results in the absence of flow for both configurations.

Figures 9a and 9b show a comparison of the educed impedances with grazing flow. Overall, the resistances obtained for the flow conditioner case are lower than those obtained for the default configuration. This pattern agrees with the model predictions, since δ^* was greater for the flow conditioner case. As mentioned before, the model presents a better agreement with the upstream source results, showing some agreement with the downstream results only for higher

frequencies. However, a good match is shown for the difference predicted by the model and seem at the experimental results, for both upstream and downstream source. The upstream results for the flow conditioner configuration present some unexpected values for the resistance in the lower frequencies, which can be explained by the absence of the anechoic terminations at the inlet, causing high acoustic reflections with flow. The reactance values exhibit good match between the two configurations.

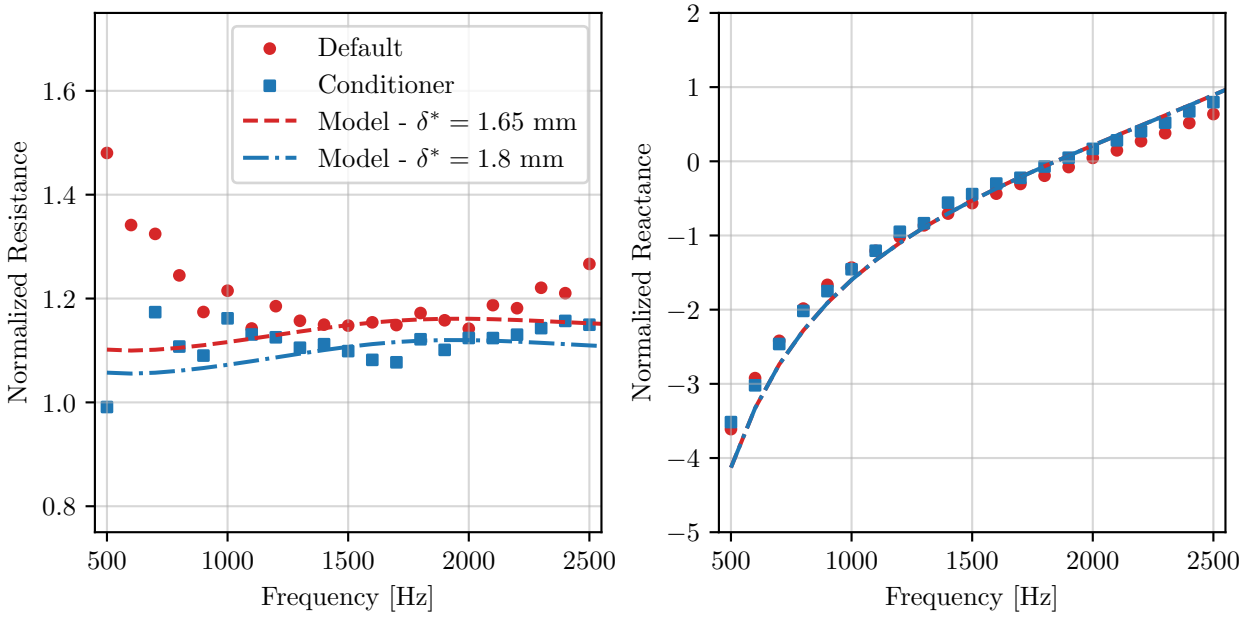

(a) Upstream source.

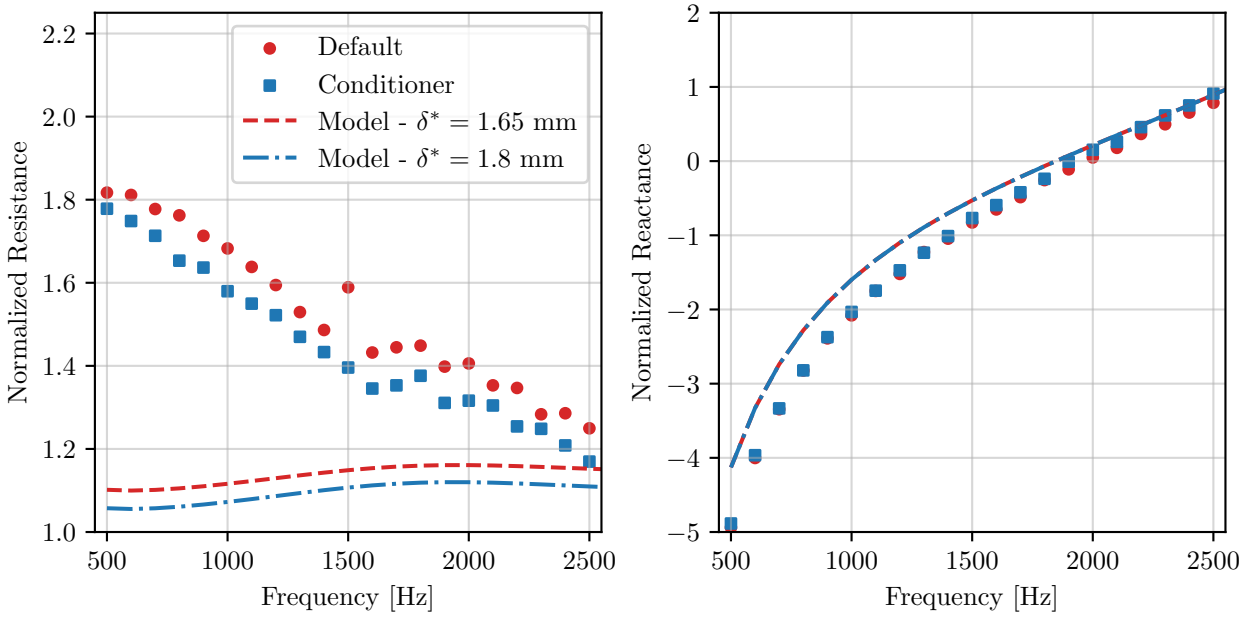

(b) Downstream source.

Fig. 9 Impedance results for the default and the flow conditioner configurations with centerline Mach number 0.3.

A more direct comparison between the model an the experimental results can be made by accounting for the differences of the boundary layers found for the two configurations. Fig. 10 presents these differences, which are the

resistance values for the lower δ^* subtracted by the values for the higher one, for the upstream, downstream source and the model. The differences obtained are rather small for the resistance values, since the changes in the displacement thickness are also small. Even for this slight change, good agreement is observed between the experimental results and the model. This suggests that the grazing flow induced resistance term of the Goodrich model is a good representation for these two cases. Discrepancies are found in the lower frequencies for the upstream source, which can be accounted for the absence of the anechoic termination.

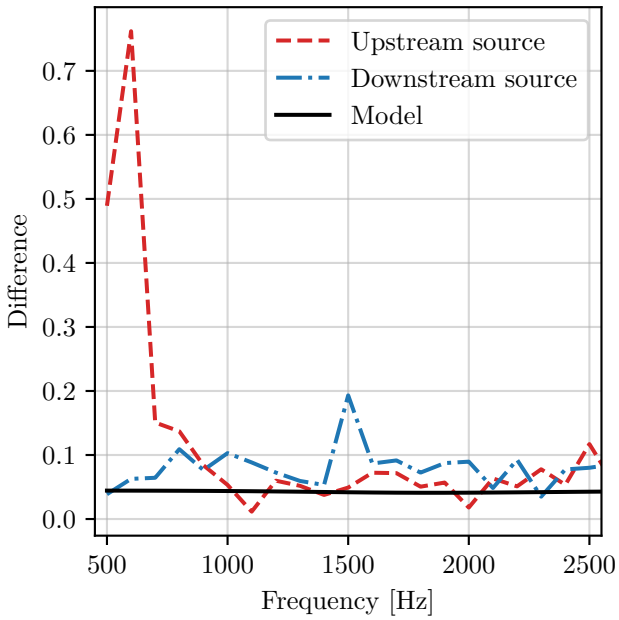

Fig. 10 Resistance difference predicted by the model and experimental

The differences between the results obtained with the different configuration follow the same pattern observed in Bonomo et al. [8]. The flow inside GFIT develops through a larger cross-section than the UFSC test rig, resulting in $\delta^* = 2.6\,\text{mm}$, higher than any configuration obtained at the UFSC test rig. Fig. 11 presents the impedance results obtained at NASA. Over most part of the frequency range, the NASA educed resistance is lower than those obtained at UFSC. Overall, the model is capable of properly predict the variation of the resistance with changes in the boundary layer displacement thickness, with the resistance decreasing as displacement thickness increases.

C. Upstream Section Configuration

A third configuration was considered by placing the sample section at the most upstream position in the test rig. Fig. 12 shows an schematic of this configuration, where all the parts upstream of the sample section were removed, and the sample section attached directly to the inlet. In this assembly, the distance between the inlet and the liner sample is very small, such that the flow is most probably not fully developed.

For this specific setup, only cases with downstream source excitation can be tested. Other configurations were tested with at least one other section included between the inlet and the liner, but they resulted in flow profiles really close to the default one. This suggests that the flow development occurs rather quickly, reaching its fully developed state after a single section of the rig.

The flow velocity measurements for this setup are presented in Fig. 13, in comparison with the results for the default setup. The new flow profile obtained is clearly under-developed, and velocities measured near the walls are higher than what is found for the default configuration, while center velocities are smaller in this case and almost constant along the mid-span. The average mach number is kept constant, $M_{\text{avg}} = 0.258$, and the displacement thickness obtained is $\delta^* = 0.9\,\text{mm}$.

Fig. 14 shows the impedance results for the default and the upstream section configurations with centerline Mach number 0.3. Results are only presented for the downstream source, given the limitations of this setup discussed before. Unlike previous results, the changes in the flow profile for this case did not have a considerable impact on the impedance

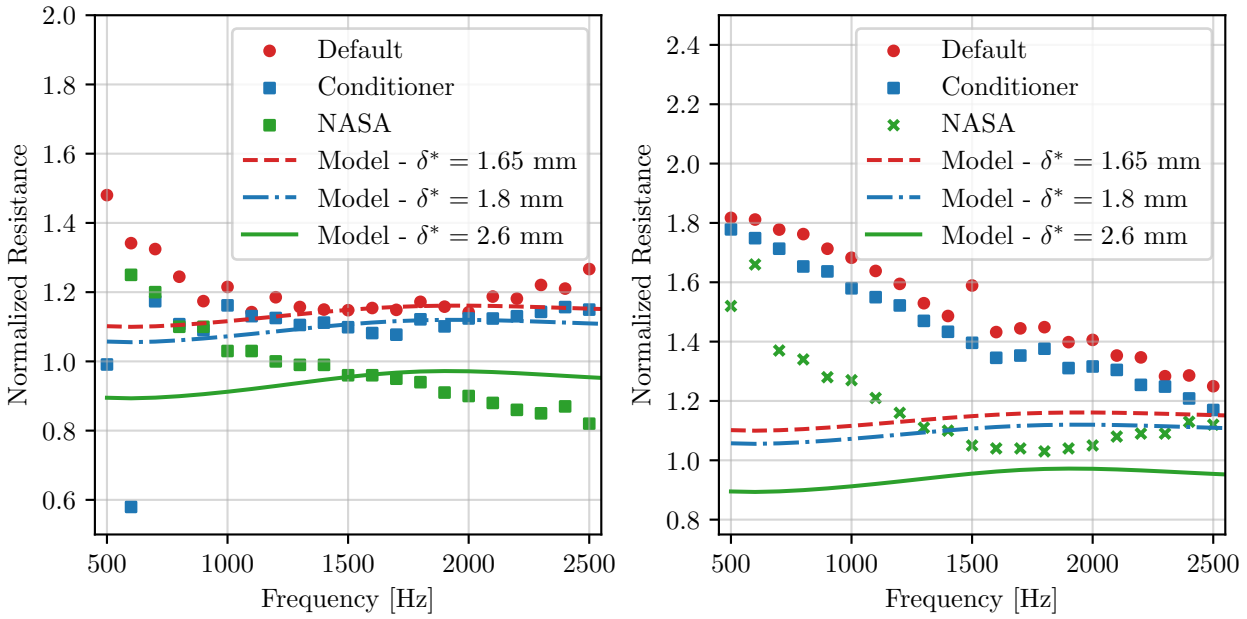

Fig. 11 Educed resistance comparison between both configurations and NASA. Left: upstream source and right: downstream source

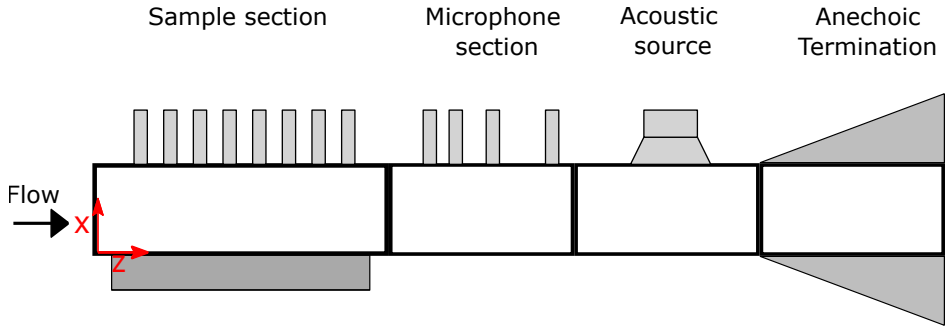

Fig. 12 Schematic of the sample section upstream configuration.

results, since both resistance and reactance presented good agreement with the default setup. For this case, the model predicted a significant increase in resistance, which is not observed in the experimental results.

The mismatch between the model and the experiments with smaller displacement thicknesses need further investigation. A reasonable hypothesis is that the flow might quickly develop along the liner sample, approximating to the original profile. Another possible explanation is that the grazing flow induced resistance term is not capable of properly predicting the resistance behavior for smaller boundary layer displacement thickness values.

V. Concluding Remarks

This paper presented a study on the effects of different boundary layer profiles on experimental impedance results. A 3D printed liner sample was tested at the UFSC Liner Test Rig, and the flow profile was evaluated at the centerline of the duct and modified by means of a flow conditioner and re-positioning of the test rig sections. A semiempirical model which accounts for boundary layer parameters was used to predict the effect of different flow profiles on the impedance. The flow obtained with the flow conditioner presented higher displacement thickness and lower resistance values, as predicted by the model. These results followed the same trend observed in a previous study where the results were compared with the NASA GFIT. The resistance decreases as the displacement thickness increases, with good agreement with the model predictions. The results obtained for the upstream section configuration were very close to those found

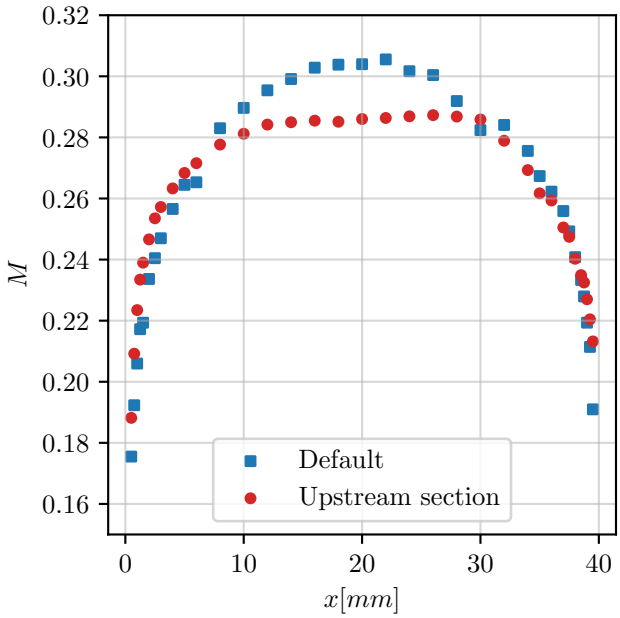

Fig. 13 Flow profiles obtained for the default and the upstream section configuration.

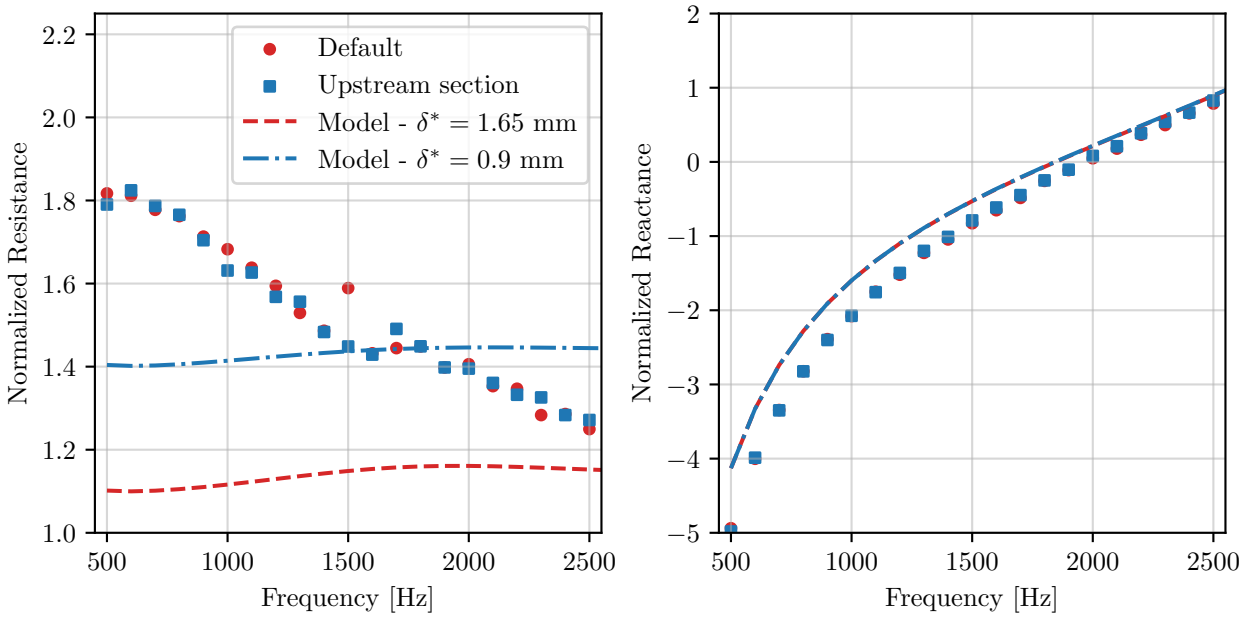

Fig. 14 Impedance results for the default and the upstream section configurations with centerline Mach number 0.3.

for the default setup, although the flow profile showed lower displacement thickness in this case. The semiempirical model did not match the experimental impedance, predicting an increase in resistance. This mismatch requires further investigations. Overall, only a few changes could be made in the boundary layer profile of the test rig, and the values of the boundary layer displacement thickness were limited to a certain range. In this sense, the duct geometry seems to be a relevant parameter when comparing different test rigs, since it leads to different boundary layer profiles.

Acknowledgments

This work was partially supported by the AeroAcoustics Research Consortium (AARC). The AARC is a government-industry partnership supporting pre-competitive research for aircraft noise reduction. N.T. Quintino, L.A. Bonomo, L.M. Pereira and J.A. Cordioli gratefully acknowledge funding from Conselho Nacional de Desenvolvimento Científico e Tecnológico (CNPq), project number 407583/2022-0. N.T. Quintino and L.M. Pereira acknowledge scholarship funding from CNPq. L.A. Bonomo acknowledges Coordenação de Aperfeiçoamento de Pessoal de Nível Superior – Brasil (CAPES) – Finance Code 001. L.A. Bonomo also acknowledges CNPq scholarship number 402701/2022-4. The work of F. Avallone is co-funded by the European Union (ERC, LINING, 101075903). Views and opinions expressed are however those of the author(s) only and do not necessarily reflect those of the European Union or the European Research Council. Neither the European Union nor the granting authority can be held responsible for them.

References

[1] Kooi, J., and Sarin, S., "An experimental study of the acoustic impedance of Helmholtz resonator arrays under a turbulent boundary layer," *7th Aeroacoustics Conference*, American Institute of Aeronautics and Astronautics, AIAA Paper 1981-1998, 1981. https://doi.org/10.2514/6.1981-1998.

[2] Murray, P., and Astley, R. J., "Development of a single degree of freedom perforate impedance model under grazing flow and high SPL," *18th AIAA/CEAS Aeroacoustics Conference (33rd AIAA Aeroacoustics Conference)*, American Institute of Aeronautics and Astronautics, AIAA Paper 2012-2294, Colorado Springs, Colorado, 2012. https://doi.org/10.2514/6.2012-2294.

[3] Jones, M., Tracy, M., Watson, W., and Parrott, T., "Effects of Liner Geometry on Acoustic Impedance," *8th AIAA/CEAS Aeroacoustics Conference & Exhibit*, American Institute of Aeronautics and Astronautics, AIAA Paper 2002-2446, Breckenridge, Colorado, 2002. https://doi.org/10.2514/6.2002-2446.

[4] Jing, X., Peng, S., and Sun, X., "A straightforward method for wall impedance eduction in a flow duct," *The Journal of the Acoustical Society of America*, Vol. 124, No. 1, 2008, pp. 227–234. https://doi.org/10.1121/1.2932256.

[5] Bake, F., Burgmayer, R., Schulz, A., Knobloch, K., Enghardt, L., and Jones, M. G., "IFAR liner benchmark challenge #1 – DLR impedance eduction of uniform and axially segmented liners and comparison with NASA results," *International Journal of Aeroacoustics*, Vol. 20, 2021, pp. 478–496. https://doi.org/10.1177/1475472X211023844/ASSET/IMAGES/LARGE/10.1177_1475472X211023844-FIG2.JPEG.

[6] Jones, M. G., Nark, D. M., and Howerton, B. M., "Overview of Liner Activities in Support of the International Forum for Aviation Research," *25 AIAA/CEAS Aeroacoustics 2022 Conference*, American Institute of Aeronautics and Astronautics, AIAA Paper 2019-2599, 2019. https://doi.org/10.2514/6.2019-2599.

[7] Boden, H., Sack, S., and Jacob, S., "Impedance measurements for 3-D printed liners," *25th AIAA/CEAS Aeroacoustics Conference*, 2019, p. 2600.

[8] Bonomo, L. A., Quintino, N. T., Cordioli, J. A., Avallone, F., Jones, M. G., Howerton, B. M., and Nark, D. M., "A Comparison of Impedance Eduction Test Rigs with Different Flow Profiles," *AIAA AVIATION 2023 Forum*, 2023, p. 3346.

[9] Yu, J., Ruiz, M., and Kwan, H. W., "Validation of Goodrich perforate liner impedance model using NASA langley test data," *14th AIAA/CEAS Aeroacoustics Conference (29th AIAA Aeroacoustics Conference)*, American Institute of Aeronautics and Astronautics, AIAA Paper 2008-2930, 2008. https://doi.org/10.2514/6.2008-2930.

[10] Ingard, U., "Influence of Fluid Motion Past a Plane Boundary on Sound Reflection, Absorption, and Transmission," *The Journal of the Acoustical Society of America*, Vol. 31, No. 7, 1959, pp. 1035–1036. https://doi.org/10.1121/1.1907805.

[11] Myers, M., "On the acoustic boundary condition in the presence of flow," *Journal of Sound and Vibration*, Vol. 71, No. 3, 1980, pp. 429 – 434. https://doi.org/10.1016/0022-460X(80)90424-1.

[12] Kumaresan, R., and Tufts, D., "Estimating the parameters of exponentially damped sinusoids and pole-zero modeling in noise," *IEEE Transactions on Acoustics, Speech, and Signal Processing*, Vol. 30, No. 6, 1982, pp. 833–840. https://doi.org/10.1109/TASSP.1982.1163974.

[13] Renou, Y., and Aurégan, Y., "Failure of the Ingard–Myers boundary condition for a lined duct: An experimental investigation," *The Journal of the Acoustical Society of America*, Vol. 130, No. 1, 2011, pp. 52–60. https://doi.org/10.1121/1.3586789.

[14] Watson, W. R., Carpenter, M. H., and Jones, M. G., "Performance of Kumaresan and Tufts algorithm in liner impedance eduction with flow," *AIAA Journal*, Vol. 53, No. 4, 2015, pp. 1091–1102. https://doi.org/10.2514/1.J053705.

[15] Bonomo, L. A., Spillere, A. M., and Cordioli, J. A., "Parametric Uncertainty Analysis for Impedance Eduction Based on Prony's Method," *AIAA Journal*, Vol. 58, 2020, pp. 3625–3638. https://doi.org/10.2514/1.J059071.

[16] "ISO 3966:2008. Measurement of fluid flow in closed conduits — Velocity area method using Pitot static tubes," manual, International Organization for Standardization, Genebra, Suíça, 2008. Tex.org-short: ISO.

[17] "ISO 12767:2007. Measurement of fluid flow by means of pressure differential devices," manual, International Organization for Standardization, Genebra, Suíça, 2007. Tex.org-short: ISO.

[18] Jones, M. G., and Nark, D. M., "Partition Thickness Considerations for Additively Manufactured Acoustic Liners," 2023.

[19] Heidelberg, L. J., Rice, E. J., and Homyak, L., "Experimental evaluation of a spinning-mode acoustic-treatment design concept for aircraft inlets," Tech. rep., 1980.

[20] Spillere, A. M. N., Bonomo, L. A., Cordioli, J. A., and Brambley, E. J., "Experimentally testing impedance boundary conditions for acoustic liners with flow: Beyond upstream and downstream," *Journal of Sound and Vibration*, Vol. 489, 2020, p. 115676. https://doi.org/10.1016/J.JSV.2020.115676.